This is the accepted manuscript made available via CHORUS. The article has been published as:

Spin-injection-induced gain anisotropy in a polariton diode laser

Aniruddha Bhattacharya and Pallab Bhattacharya

Phys. Rev. B **97**, 085202 — Published 14 February 2018

DOI: 10.1103/PhysRevB.97.085202

Spin-injection-induced Gain Anisotropy in a Polariton Diode Laser

Aniruddha Bhattacharya and Pallab Bhattacharya*

Solid-State Electronics Laboratory, Department of Electrical Engineering and Computer Science, University of Michigan,
1301 Beal Avenue, Ann Arbor, Michigan 48109-2122, USA

*Electronic mail: pkb@umich.edu

ABSTRACT

Optical effects arising from spin-induced gain anisotropy such as threshold reduction and emission intensity enhancement, hitherto unobserved in electrically injected polariton lasers, are theoretically predicted for a bulk GaN-based exciton-polariton diode laser operated with electrical injection of spin-polarized electrons. These phenomena are deduced from a simplified spin-dependent rate equation model. We also demonstrate an electrical excitation scheme, which can amplify the degree of a deterministic circular polarization of the output emission by an order of magnitude, compared to the injected electron spin polarization, above threshold.

I. INTRODUCTION

An exciton-polariton laser is a microcavity light source where coherent photons are emitted from a non-equilibrium and degenerate polariton condensate by spontaneous emission in the strong coupling regime of exciton-photon interaction [1, 2]. Stimulated polariton-polariton scattering [3] is the relevant phase-coherent optical gain mechanism in these devices. The separation of the processes of bosonic final-state stimulation and emission leads to coherent emission without the need for population inversion [4], as in a conventional photon laser, and therefore the threshold pump level is considerably smaller [5]. This has been amply demonstrated in optically and electrically pumped polariton lasers realized with several materials and semiconductor heterostructures [1-2, 5-18]. The output polarization in the steady state, above threshold, can be linear or circular, or a combination of both, depending on the nature of the excitation [19-24], defect-induced pinning and static disorder in the microcavity [25-26], TE-TM splitting of the excitonic pseudospins [27], and injection density [25]. Spontaneous stochastic circular polarization has also been observed in GaAs-based polariton condensates at low temperatures [28].

On the other hand, we have recently demonstrated that a controlled and variable circularly polarized output can be obtained by injecting spin-polarized electrons in a polariton diode laser [29]. The magnitude and helicity of the output circular polarization is deterministically governed by the in-plane magnetization of the ferromagnetic contacts. Preferential injection of spin-polarized carriers leads to a differential population of exciton pseudospins and it is the relative spin relaxation rates compared to the polariton scattering rates that ultimately determine the nature and evolution of the polarization of the optical output as a function of excitation. In the present study, we have investigated the individual polarized

components of the output in detail in the context of spin-induced gain anisotropy (anisotropy in stimulated scattering rate) in the polariton condensate. The gain anisotropy gives rise to hitherto unidentified effects such as threshold lowering of the preferred polarization mode and enhancement of the output emission intensity at and beyond the threshold. The calculated data have been compared with measured ones, where possible. We have also examined the dynamical behavior of the output polarization components for the first time by using the relevant spin-dependent rate equation model. Spontaneous magnetization in a GaAs-based exciton-polariton condensate has been previously demonstrated; wherein condensates spontaneously emerge in either of two discrete spin-polarized states, which emit highly circularly polarized coherent light (up to ~ 95%) [28]. Although this is a remarkable observation, nevertheless the output circular polarization is essentially stochastic and uncontrolled. Here, we show for the first time, a simple and elegant mechanism to generate highly circularly polarized emission at room temperature in GaN-based condensates, which is deterministic and thus amenable to external manipulation. The helicity is controlled exclusively by the magnetization of the electron spin injector. We observe high frequency relaxation oscillations in the output, which result from the dynamic exchange of energy between carriers and exciton-polaritons, for the two polarization components. Our study reveals that very high output circular polarizations, close to 100 %, can be obtained with a modulated biasing scheme, even with rather modest values of injected electron spin polarization such as ~ 8 %, which are practically feasible at room temperature [30].

II. SPIN-DEPENDENT RATE EQUATION MODEL

We have recently reported the output optical characteristics of electrically pumped bulk GaN-based spin-polarized microcavity polariton lasers [29]. These double heterostructure edge-emitting microcavity diodes with side-clad dielectric Bragg reflector (DBR) mirrors and vertical

current injection are characterized by a typical emission wavelength $\lambda \sim 365$ nm. Typical values for the cavity-to-exciton detuning Δ and the vacuum-field Rabi splitting Ω_{VRS} in these devices are ~ -7.5 meV and ~ 36.1 meV, respectively. An important objective of the work was the study of the evolution of the steady-state output circular polarization with injection. The degree of circular polarization of the lower-polariton (LP) emission in the normal direction ($k_{||} \sim 0$) was measured as a function of injection current after the application of a suitable in-plane magnetizing field to the n-type FeCo/MgO spin injector. The measurements were made in remanence, with the magnetic field switched off, with continuous-wave (CW) current injection. Figure 1(a) shows the circular-polarization resolved lower-polariton (LP) occupation numbers measured as a function of injection after magnetization of the contacts with $H \sim +1.6$ kOe. These ground-state occupancies are estimated by normalizing to unity the recorded electroluminescence intensities for each of the helicities, at their respective thresholds. The inset of Fig. 1(a) depicts the measured steady state circular polarization of the output LP electroluminescence as a function of injection, deduced from the data of Fig. 1(a). There is a non-linear increase of the polarization at threshold and a maximum value of output circular polarization of ~ 25 % is observed above the non-linear threshold. These experimental data have been reported by us in a previous publication [29]. Experimental data describing the strong coupling regime of operation of the devices and their output spectral characteristics, such as the emission linewidth and blueshift of the peak emission energy, have been reported in Ref. [29].

We have analyzed the measured circular polarization results with the object of investigating the magnification of the injected spin polarization due to the bosonic stimulation effect, using a spin-dependent rate equation model. This rate equation model has been devised following Iorsh et al. [31], wherein they present a simplified quasi-analytic model for GaN-based

polariton lasers. We assume that the injected electrons are partially spin polarized. We solve the following rate equations for free carriers, excitons and exciton-polaritons, taking into account both of their respective spin projections along the axis of light emission:

$$\frac{dN_{eh}^{\uparrow}}{dt} = \xi\frac{\vec{J}.\vec{S}}{q} - \frac{N_{eh}^{\uparrow}}{\tau_{eh}} - WN_{eh}^{\uparrow} + \left(\frac{N_{eh}^{\downarrow} - N_{eh}^{\uparrow}}{\tau_{s,e}}\right) \quad (1)$$

$$\frac{dN_{eh}^{\downarrow}}{dt} = (1-\xi)\frac{\vec{J}.\vec{S}}{q} - \frac{N_{eh}^{\downarrow}}{\tau_{eh}} - WN_{eh}^{\downarrow} - \left(\frac{N_{eh}^{\downarrow} - N_{eh}^{\uparrow}}{\tau_{s,e}}\right) \quad (2)$$

$$\frac{dN_R^{\uparrow}}{dt} = -\frac{N_R^{\uparrow}}{\tau_R} + \left(\frac{N_R^{\downarrow} - N_R^{\uparrow}}{\tau_{s,R}}\right) + WN_{eh}^{\uparrow} - aN_R^{\uparrow}(N_P^{\uparrow}+1) + ae^{-\beta\Delta_{esc}}N_P^{\uparrow}N_R^{\uparrow} - b(N_R^{\uparrow})^2(N_P^{\uparrow}+1) - cN_{eh}^{\uparrow}N_R^{\uparrow}(N_P^{\uparrow}+1) \quad (3)$$

$$\frac{dN_R^{\downarrow}}{dt} = -\frac{N_R^{\downarrow}}{\tau_R} - \left(\frac{N_R^{\downarrow} - N_R^{\uparrow}}{\tau_{s,R}}\right) + WN_{eh}^{\downarrow} - aN_R^{\downarrow}(N_P^{\downarrow}+1) + ae^{-\beta\Delta_{esc}}N_P^{\downarrow}N_R^{\downarrow} - b(N_R^{\downarrow})^2(N_P^{\downarrow}+1) - cN_{eh}^{\downarrow}N_R^{\downarrow}(N_P^{\downarrow}+1) \quad (4)$$

$$\frac{dN_P^{\uparrow}}{dt} = -\frac{N_P^{\uparrow}}{\tau_P} + aN_R^{\uparrow}(N_P^{\uparrow}+1) - ae^{-\beta\Delta_{esc}}N_P^{\uparrow}N_R^{\uparrow} + b(N_R^{\uparrow})^2(N_P^{\uparrow}+1) + cN_{eh}^{\uparrow}N_R^{\uparrow}(N_P^{\uparrow}+1) + \gamma(N_P^{\downarrow} - N_P^{\uparrow}) \quad (5)$$

$$\frac{dN_P^{\downarrow}}{dt} = -\frac{N_P^{\downarrow}}{\tau_P} + aN_R^{\downarrow}(N_P^{\downarrow}+1) - ae^{-\beta\Delta_{esc}}N_P^{\downarrow}N_R^{\downarrow} + b(N_R^{\downarrow})^2(N_P^{\downarrow}+1) + cN_{eh}^{\downarrow}N_R^{\downarrow}(N_P^{\downarrow}+1) - \gamma(N_P^{\downarrow} - N_P^{\uparrow}) \quad (6)$$

Here $N_{eh}^{\uparrow}$, $N_{eh}^{\downarrow}$, $N_R^{\uparrow}$, $N_R^{\downarrow}$, $N_P^{\uparrow}$ and $N_P^{\downarrow}$ are the electron, exciton reservoir and ground-state lower-polariton occupation numbers corresponding to spin-up and spin-down electron states, respectively, ξ is the pump current spin polarization assumed to be ~ 60 %, J is the injected current density, S is the cross-sectional area of the active region of the microcavity diode having dimensions of 690 nm by 40 μm, $W \sim 10000$ ps^{-1} is the excitonic formation rate, $\tau_{s,e} \sim 40$ ps is

the electron spin relaxation time [30], $\tau_{eh} \sim 2000$ ps is the total electron-hole recombination lifetime, $\tau_R = 1$ ns is the exciton non-radiative recombination time, $\tau_{s,R} \sim 120$ ps is the excitonic pseudospin relaxation time, $a \sim 10^{-7}$ ps^{-1}, $b \sim 10^{-9}$ ps^{-1}, $c \sim 10^{-14}$ ps^{-1} are the phonon-polariton, polariton-polariton and polariton-electron scattering rates, $\beta = 1/k_BT$, $\Delta_{esc} \sim 20$ meV is the trap depth of the LP branch, $\tau_c \sim 1$ ps is the polariton lifetime, and $\gamma \sim 0.035$ ps^{-1} is the effective spin relaxation for the lower-polaritons at the band bottom. We define the pump current spin polarization $\xi = (1 + P_{spin})/2$, where P_{spin} is the injected electron spin polarization. This definition is also consistent with the formalism in Ref. [29]. Thus, an injected electron spin polarization of 8 % ($P_{spin} = 0.08$) translates to a pump current spin polarization of 54 % ($\xi = 0.54$). Further, to theoretically incorporate the effects of non-idealities in the device performance, principally nonradiative recombination and carrier leakage from the active recombination region, we have introduced a damping factor for the electrical excitation. Replacing J by J^{η} where $\eta \sim 0.7$, gives best agreement to our measured data. This is consistent with our previous analysis of the sub-threshold regime of the polariton light-current characteristics in similar devices [18]. The calculated variation of the circular polarization-resolved light-current characteristics is shown alongside the measured data in Fig. 1(a) and a good agreement is observed. It has been reported, that because of the various uncertainties in the process of estimation, there can be up to one order of magnitude uncertainty in the ground-state polariton occupations at threshold which explains the observed discrepancy below threshold [5]. The agreement of the measured output circular polarization data with calculated values is shown in the inset of Fig. 1(a).

The excitonic formation term is non-linear in the present model as well as in the one presented in Ref. [29]. Here, we have used the total unbound electron-hole plasma occupation

number as a single quantity, instead of individual electron and hole densities, and thus this term in equations (1) and (2) appears to be linear. Other significant differences between the two formalisms include the inclusion of terms accounting for polariton-electron scattering and phonon-assisted depopulation of the polariton ground state in the present work. There is an appreciable variation in the values of some of the parameters, especially those corresponding to the excitonic terms, in the present theoretical model as compared to those in the coupled stochastic differential equation model of Ref. [29]. We believe that the reason may be a complex interplay of the different terms which have been included in each of the models. Further, in the coupled stochastic differential equation approach, a complex additive white Gaussian noise term is usually introduced to explicitly describe symmetry breaking. This has been both theoretically discussed [32] as well as experimentally confirmed in the literature [25, 26]. In the present study, we have used a simplified approach, which results in a smooth variation of the calculated parameters, such as of the ground-state occupations as a function of excitation.

III.SPIN-INDUCED GAIN ANISOTROPY

In Fig. 1(b), we study the two contrasting cases, wherein all the above parameters are kept identical, and the magnitude of the pump current (injected electron) spin polarization is increased to 100 % (100 %) and decreased to 50 % (0 %), respectively. Even with 100 % spin polarization of the CW pump current, a maximum steady-state degree of circular polarization of ~ 90 % is calculated. This motivated us to explore alternate biasing schemes to enhance the output polarization to almost unity, even when using small values for the pump current spin polarization such as ~ 60 %, which are practically realizable in these devices. It is important to note that a reduction in the threshold for the right-hand circularly polarized (RHCP) component with 100 % pump current spin polarization is observed in Fig. 1(b). We have thus subsequently

examined the dependence of the polariton laser thresholds, for both helicities, as a function of the pump current spin polarization. We define the condensation threshold as the value of the injected current density at which the total ground-state polariton occupation ($k_{||} \sim 0$) becomes unity. The same definition applies for each of the individual spin-polarized components of the ground state. As seen in Fig. 2(a), with increasing value of the pump current spin polarization, the polariton laser thresholds for the two polarizations are further separated. This is a direct evidence of spin-induced gain anisotropy in a polariton laser operated with electrical spin injection. We define threshold reduction as the reduction in the threshold of the preferred polarization mode with respect to the threshold of an exactly equivalent polariton laser operated with no net spin injection. A maximum reduction of 10.2 A/cm^2 (~ 10 %) is predicted for operation with 100 % pump current spin polarization, assuming all other device parameters remain unchanged. We note that for operation with ~ 60 % pump current spin polarization, we calculate a difference of ~ 5 A/cm^2, between the thresholds for the two helicities, which we were unable to clearly observe in our measured data. We attribute this to the uncertainties in the magnitudes of the LP electroluminescence intensities at or near threshold due to measurement error, which lead to difficulties in the assignment of threshold exactly from light (output)-current characteristics. Further, it has been reported by other groups that in GaN-based microcavities there can be several factors, which contribute to errors in the process of estimation of the $k_{||} \sim 0$ occupancies, directly from the data for zero emission angle [9]. The above-mentioned phenomenon of threshold reduction for the two different circular polarizations has been previously experimentally observed in optically excited polariton lasers [33, 34]. However, an external magnetic field in the Faraday geometry, instead of injection of spin-polarized electrons, was used

to induce spin anisotropy by inducing LP condensation in the lower of the two Zeeman-split spin states.

Because of spin-induced gain anisotropy and the resulting threshold reduction, a spin polariton laser is expected to exhibit an increase in the total optical power for a given bias current under spin-polarized pumping. Here, we define the emission intensity enhancement as $\Delta S = (S-S_0)/S_0$, where S (S_0) is the total light intensity output for a polariton laser operated with spin-polarized (conventional) electrical injection. Figure 2(b) shows the non-linear increase of the emission intensity enhancement, ΔS, above the polariton laser threshold when operated with 100 % pump current spin polarization. A maximum enhancement of ~ 8.5 % is theoretically predicted above threshold. The inset shows the calculated total light (output)-current characteristics for operation with 100 % and 0 % injected electron spin polarizations respectively, from which the percentage of enhancement of the total electroluminescence on switching from 0 % to 100 % electron spin polarization, as a function of the injected current density, has been determined.

IV.TEMPORAL BEHAVIOR OF POLARIZATION

Finally, we examine the temporal evolution of the circular polarization in the output emission. In Fig. 3(a), we time resolve the occupation numbers of the two spin components under the influence of a unit step response. All the parameters in our calculations are kept identical to those used to analyze the data in Fig. 1(a). We choose a suitable excitation level above the polariton laser threshold (~ 2 kA/cm^2), where the strong-coupling characteristics are still maintained, and at which relaxation oscillations in the output circular polarization become evident. The oscillations in the polariton occupations are mainly due to the polariton spin

relaxation mechanisms, which bring about an exchange of polaritons between the two opposite circular polarizations, and other scattering processes. The fact that the oscillations are out of phase is a direct consequence of seeding the ground-state with an initial spin imbalance originating from the electron spin injection process, which eventually leads to a higher steady-state oscillation amplitude for the preferred polarization component. The large amplitude of the relaxation oscillation of the degree of circular polarization (~ 85 %) seen in the inset is promising in that it can be efficiently measured with a periodic biasing scheme. To that end, the laser is electrically excited with a high-frequency periodic square wave pulse train. The period of the excitation is chosen to be 2 ns, from the calculated temporal decay in Fig. 3(a). A duty cycle of ~ 10 % is found to give the best results, preventing any appreciable undershoot of the degree of circular polarization during the time-period when the pulse is active, thus giving rise to a large positive magnitude of the circular polarization. As shown in Fig. 3(b), we observe a large value for the degree of output circular polarization (~ 82.5 %), even when operating with an injected electron spin polarization of ~ 8 %, a ten-fold enhancement in the process of transduction of the injected electron spin angular momentum to the circular spin polarization of the coherently emitted photon. A detector, operated synchronously with the excitation source, will be able to sample the strongly polarized output generated after the initiation of every pulse, with the sampling carried out for a period of ~ 250 ps after the commencement of every new cycle. The inset shows the temporal variation of the two LP components, under these excitation conditions.

V. CONCLUSION

In conclusion, we have investigated the output intensity and polarization characteristics of a GaN-based microcavity spin-polarized polariton diode laser in which spin-polarized electrons are injected. Measured data on these devices have been analyzed and theoretical

calculations based on a spin-dependent rate equation model have been made. Threshold reduction and enhancement of the output emission as a function of spin injection are demonstrated for the first time. More importantly, the temporal characteristics of the output intensity and circular polarization have been determined and a novel biasing scheme of measuring ~ 100 % output polarization with less than 10 % spin injection is presented. Such a compact low-power coherent light source with a controllable highly circularly polarized output would be useful for many applications.

Acknowledgements

The work is supported by the National Science Foundation under the Materials Research Science and Engineering Center (MRSEC) program (Grant No. DMR-1120923).

References:

1. H. Deng, G. Weihs, C. Santori, J. Bloch, and Y. Yamamoto, Science **298**, 199 (2002).
2. H. Deng, G. Weihs, D. Snoke, J. Bloch, and Y. Yamamoto, Proc. Natl. Acad. Sci. U. S. A. **100**, 15318 (2003).
3. P. G. Savvidis, J. J. Baumberg, R. M. Stevenson, M. S. Skolnick, D. M. Whittaker, and J. S. Roberts, Phys. Rev. Lett. **84**, 1547 (2000).
4. D. Solnyshkov, E. Petrolati, A. Di Carlo, and G. Malpuech, Appl. Phys. Lett. **94**, 011110 (2009).
5. P. Bhattacharya, B. Xiao, A. Das, S. Bhowmick, and J. Heo, Phys. Rev. Lett. **110**, 206403 (2013).
6. Le Si Dang, D. Heger, R. André, F. Bœuf, and R. Romestain, Phys. Rev. Lett. **81**, 3920 (1998).
7. J. Kasprzak, M. Richard, S. Kundermann, A. Baas, P. Jeambrun, J. M. J. Keeling, F. M. Marchetti, M. H. Szyman´ska, R. Andre´, J. L. Staehli, V. Savona, P. B. Littlewood, B. Deveaud, and Le Si Dang, Nature **443**, 409 (2006).
8. R. Balili, V. Hartwell, D. Snoke, L. Pfeiffer, and K. West, Science **316**, 1007 (2007).

9. S. Christopoulos, G. B. H. von Hogersthal, A. J. D. Grundy, P. G. Lagoudakis, A. V. Kavokin, J. J. Baumberg, G. Christmann, R. Butte, E. Feltin, J.-F. Carlin, and N. Grandjean, Phys. Rev. Lett. **98**, 126405 (2007).
10. S. Kena-Cohen and S. R. Forrest, Nat. Photonics **4**, 371 (2010).
11. D. Bajoni, P. Senellart, E. Wertz, I. Sagnes, A. Miard, A. Lemaitre, and J. Bloch, Phys. Rev. Lett. **100**, 047401 (2008).
12. G. Christmann, R. Butte, E. Feltin, J. Carlin, and N. Grandjean, Appl. Phys. Lett. **93**, 051102 (2008).
13. M. Nomura, N. Kumagai, S. Iwamoto, Y. Ota, and Y. Arakawa, Nat. Phys. **6**, 279 (2010).
14. A. Das, J. Heo, M. Jankowski, W. Guo, L. Zhang, H. Deng, and P. Bhattacharya, Phys. Rev. Lett. **107**, 066405 (2011).
15. A. Das, J. Heo, A. Bayraktaroglu, W. Guo, T.-K. Ng, J. Phillips, B. S. Ooi, and P. Bhattacharya, Opt. Express **20**, 11 830 (2012).
16. Feng Li, L. Orosz, O. Kamoun, S. Bouchoule, C. Brimont, P. Disseix, T. Guillet, X. Lafosse, M. Leroux, J. Leymarie, M. Mexis, M. Mihailovic, G. Patriarche, F. Réveret, D. Solnyshkov, J. Zuniga-Perez, and G. Malpuech, Phys. Rev. Lett. **110**, 196406 (2013).
17. P. Bhattacharya, T. Frost, S. Deshpande, M. Z. Baten, A. Hazari, and A. Das, Phys. Rev. Lett. **112**, 236802 (2014).
18. Y. Sun, P. Wen, Y. Yoon, G. Liu, M. Steger, L. N. Pfeiffer, K. West, D. W. Snoke, and K. A. Nelson, Phys. Rev. Lett. **118**, 016602 (2017).
19. M. D. Martín, G. Aichmayr, L. Viña, and R. André, Phys. Rev. Lett. **89**, 077402 (2002).
20. I. Shelykh, K. V. Kavokin, A. V. Kavokin, G. Malpuech, P. Bigenwald, H. Deng, G. Weihs, and Y. Yamamoto, Phys. Rev. B **70**, 035320 (2004).

21. D. N. Krizhanovskii, D. Sanvitto, I. A. Shelykh, M. M. Glazov, G. Malpuech, D. D. Solnyshkov, A. Kavokin, S. Ceccarelli, M. S. Skolnick, and J. S. Roberts, Phys. Rev. B **73**, 073303 (2006).
22. G. Roumpos, C.-W. Lai, T. C. H. Liew, Y. G. Rubo, A. V. Kavokin, and Y. Yamamoto, Phys. Rev. B **79**, 195310 (2009).
23. A. Amo, T. C. H. Liew, C. Adrados, R. Houdré, E. Giacobino, A. V. Kavokin, and A. Bramati, Nature Photon. **4**, 361 (2010).
24. H. Ohadi, E. Kammann, T. C. H. Liew, K. G. Lagoudakis, A. V. Kavokin, and P. G. Lagoudakis, Phys. Rev. Lett. **109**, 016404 (2012).
25. J. Levrat, R. Butté, T. Christian, M. Glauser, E. Feltin, J.-F. Carlin, N. Grandjean, D. Read, A. V. Kavokin, and Y. G. Rubo, Phys. Rev. Lett. **104**, 166402 (2010).
26. A. Bhattacharya, M. Z. Baten, I. Iorsh, T. Frost, A. Kavokin, and P. Bhattacharya, Phys. Rev. B **94**, 035203 (2016).
27. G. Panzarini, L. C. Andreani, A. Armitage, D. Baxter, M. S. Skolnick, V. N. Astratov, J. S. Roberts, A. V. Kavokin, M. R. Vladimirova, and M. A. Kaliteevski, Phys. Rev. B **59**, 5082 (1999).
28. H. Ohadi, A. Dreismann, Y.□G. Rubo, F. Pinsker, Y. del Valle-Inclan Redondo, S.□I. Tsintzos, Z. Hatzopoulos, P.□G. Savvidis, and J.□J. Baumberg, Phys. Rev. X **5**, 031002 (2015).
29. A. Bhattacharya, M. Z. Baten, I. Iorsh, T. Frost, A. Kavokin, and P. Bhattacharya, Phys. Rev. Lett. **119**, 067701 (2017).
30. A. Bhattacharya, M. Z. Baten, and P. Bhattacharya, Appl. Phys. Lett. **108**, 042406 (2016).

31. I. Iorsh, M. Glauser, G. Rossbach, J. Levrat, M. Cobet, R. Butte, N. Grandjean, M. A. Kaliteevski, R. A. Abram, and A. V. Kavokin, Phys. Rev. B **86**, 125308 (2012).
32. D. Read, T. C. H. Liew, Yuri G. Rubo, and A. V. Kavokin, Phys. Rev. B **80**, 195309 (2009).
33. C. Sturm, D. Solnyshkov, O. Krebs, A. Lemaître, I. Sagnes, E. Galopin, A. Amo, G. Malpuech, and J. Bloch, Phys. Rev. B **91**, 155130 (2015).
34. J.-G. Rousset, B. Piętka, M. Król, R. Mirek, K. Lekenta, J. Szczytko, W. Pacuski, and M. Nawrocki, Phys. Rev. B **96**, 125403 (2017).

Figure Captions

Figure 1 (color online) (a) Circular polarization-resolved lower-polariton (LP) occupation numbers, measured along angle of zero emission ($k_{||} \sim 0$), as a function of injected current density recorded after in-plane magnetization of ferromagnetic contacts with H ~ + 1.6 kOe. The solid blue (brown) line represents the calculated light-current characteristics for the right (left)-circularly polarized components, respectively. The vertical green arrow indicates the onset of non-linearity. The inset shows the measured steady-state degree of circular polarization as a function of injected current density. The green solid line, in the inset, represents the calculated polarization values; (b) circular polarization-resolved lower-polariton (LP) occupation numbers, calculated for zero angle of emission ($k_{||} \sim 0$), as a function of injected current density, for 100 % and 0 % injected electron spin polarizations, respectively. The solid blue (green) line represent the calculated light-current characteristics for the right (left)-circularly polarized components, respectively. The solid brown curve and the coincident solid black curve represent the two

identical circular polarization-resolved light-current characteristics of a polariton laser diode operated with no net electron spin injection.

Figure 2 (color online) (a) Variation of the calculated polariton laser thresholds for each of the individual helicities, and the reduction in the threshold for the preferred polarization component (right-hand circularly polarized) with respect to that for operation without spin injection, as a function of the pump current spin polarization. The errors bars represent the uncertainties in the process of estimation of the threshold reduction, originating from the resolution of current density used in our calculations; (b) percentage of enhancement of the total electroluminescence on switching from 0 % to 100 % electron spin polarization, as a function of the injected current density. The inset shows the two light-current characteristics plotted in a double linear scale, to clearly depict the separation in the two, effected by the process of electron spin injection.

Figure 3 (color online) (a) Calculated temporal evolution of the spin-up and spin-down lower-polariton (LP) occupation numbers for the case of electrical excitation with a 2 kA/cm^2 step function. The inset shows the corresponding evolution of the degree of the output circular polarization under identical conditions; (b) calculated variation of the degree of the output circular polarization, as a function of time, for the case of excitation with a periodic square pulse having a peak amplitude of 2 kA/cm^2. The biasing pulse has a period of 2 ns and a duty cycle of 10 %. The inset shows the corresponding variation of the two LP components with time.

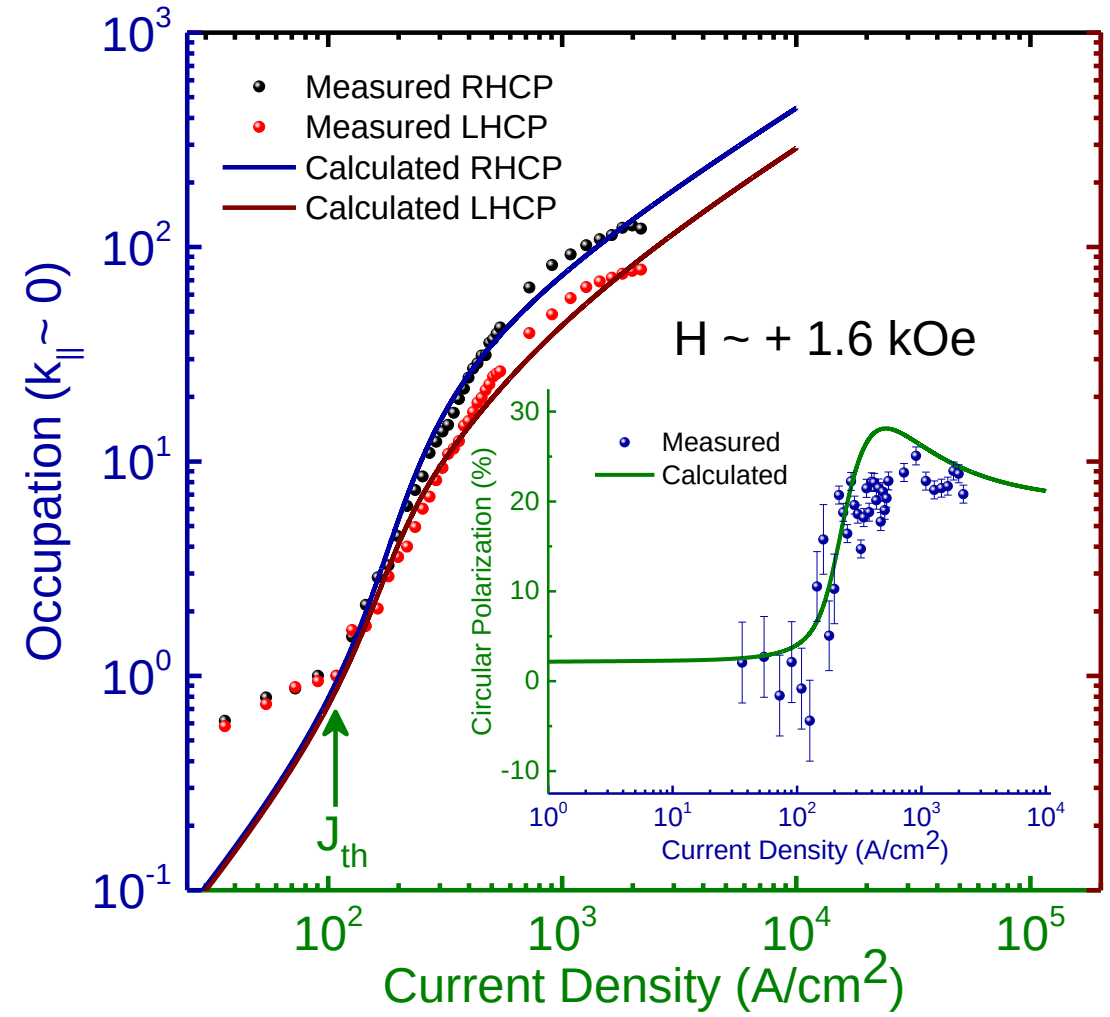

(a)

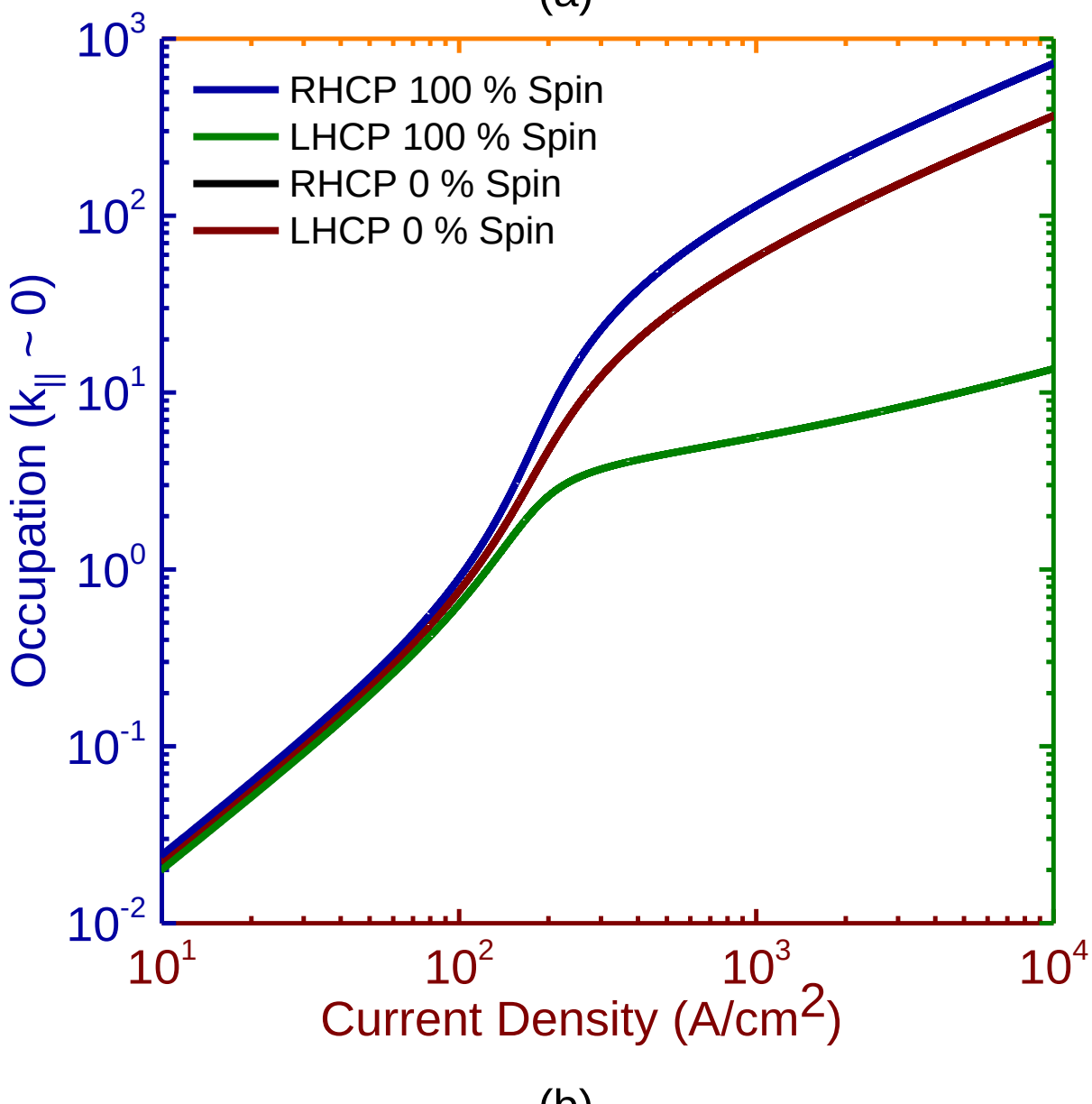

(b)

Figure 1 of 3

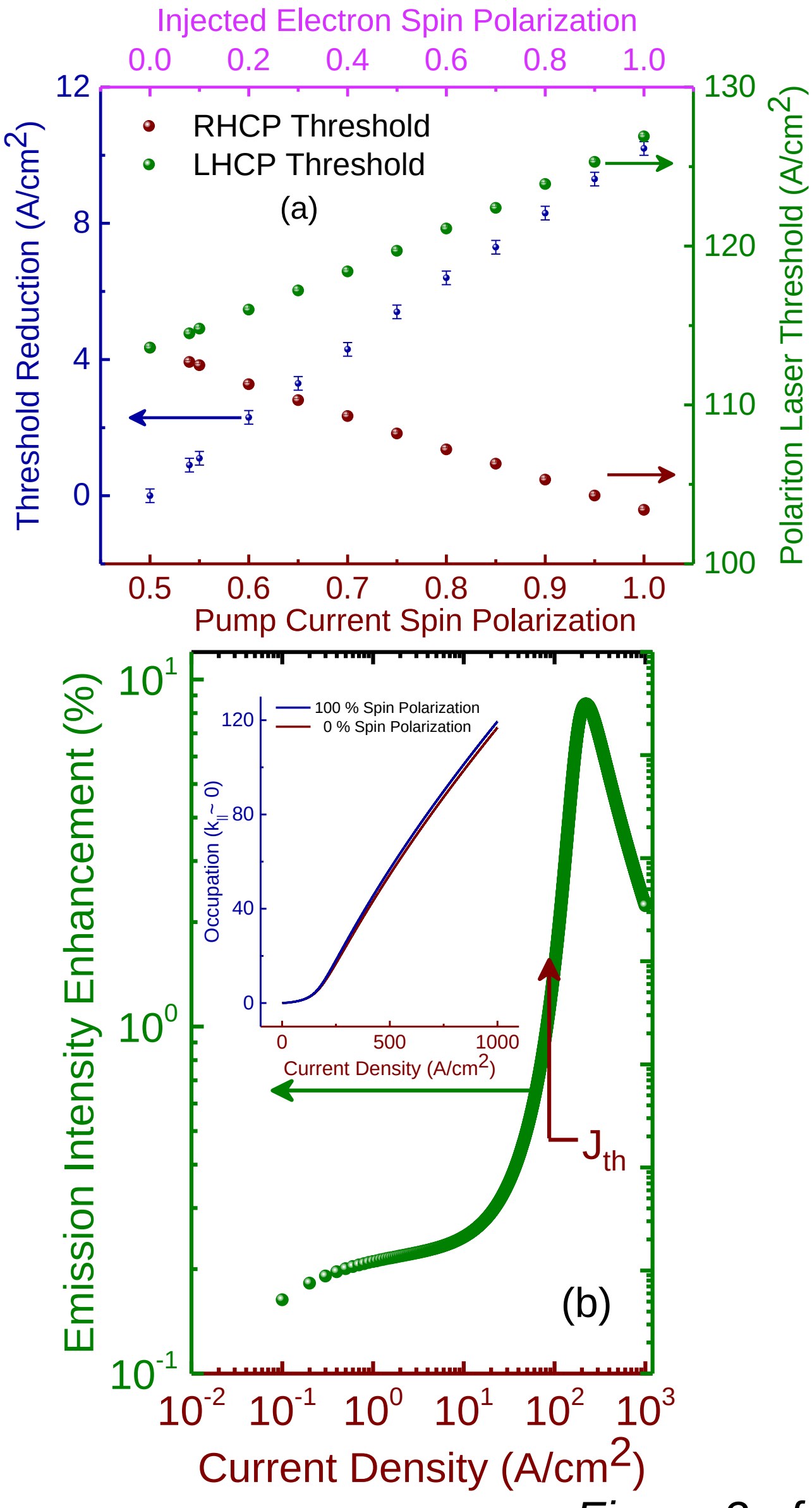
Injected Electron Spin Polarization
0.0
0.2
0.4
0.6
0.8
1.0
RHCP Threshold
LHCP Threshold
(a)
Threshold Reduction (A/cm2)
Polariton Laser Threshold (A/cm2)
Pump Current Spin Polarization
100 % Spin Polarization
0 % Spin Polarization
Occupation (k|| ~ 0)
Current Density (A/cm2)
Jth
(b)
Emission Intensity Enhancement (%)
Current Density (A/cm2)

Figure 2 of 3

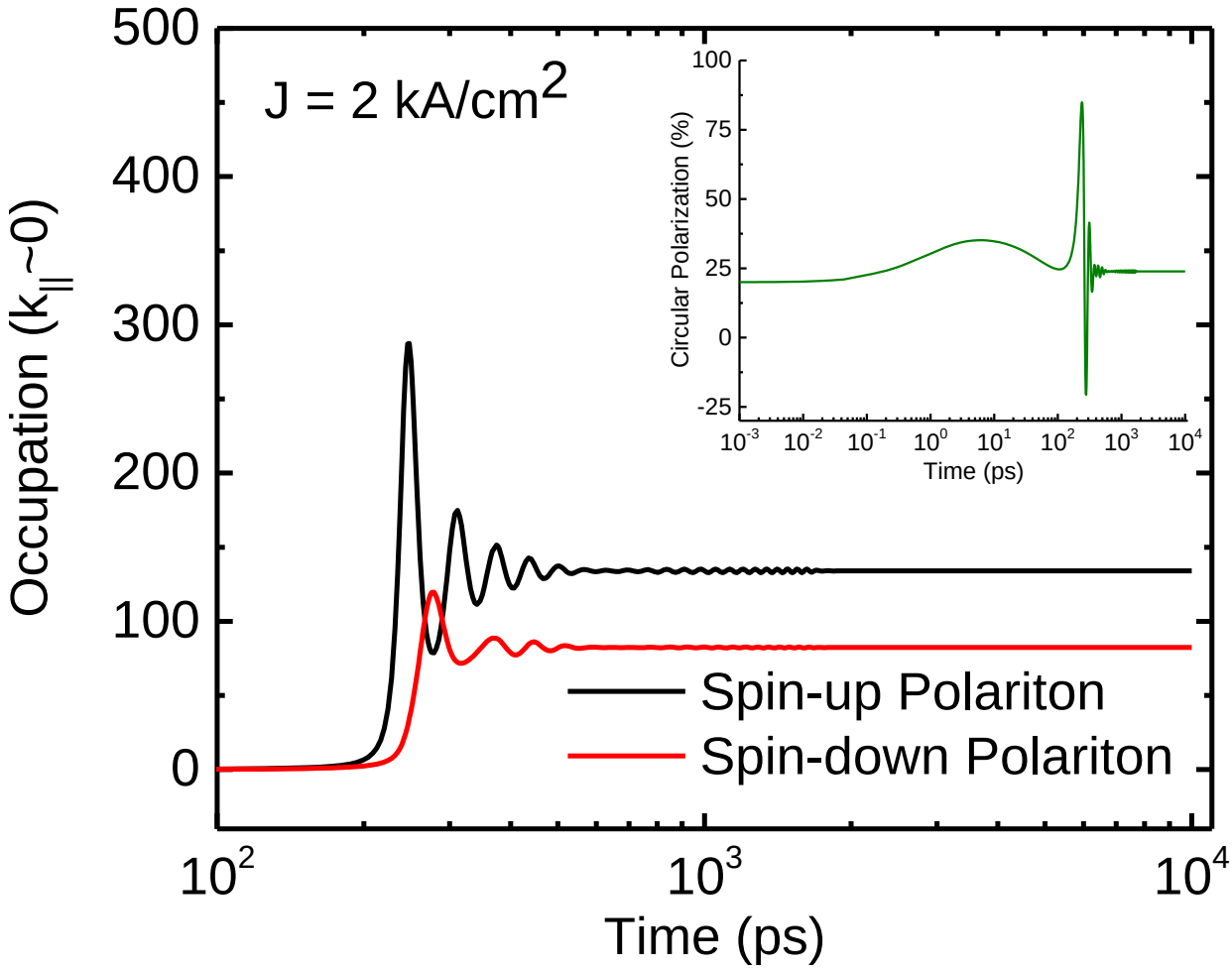

(a)

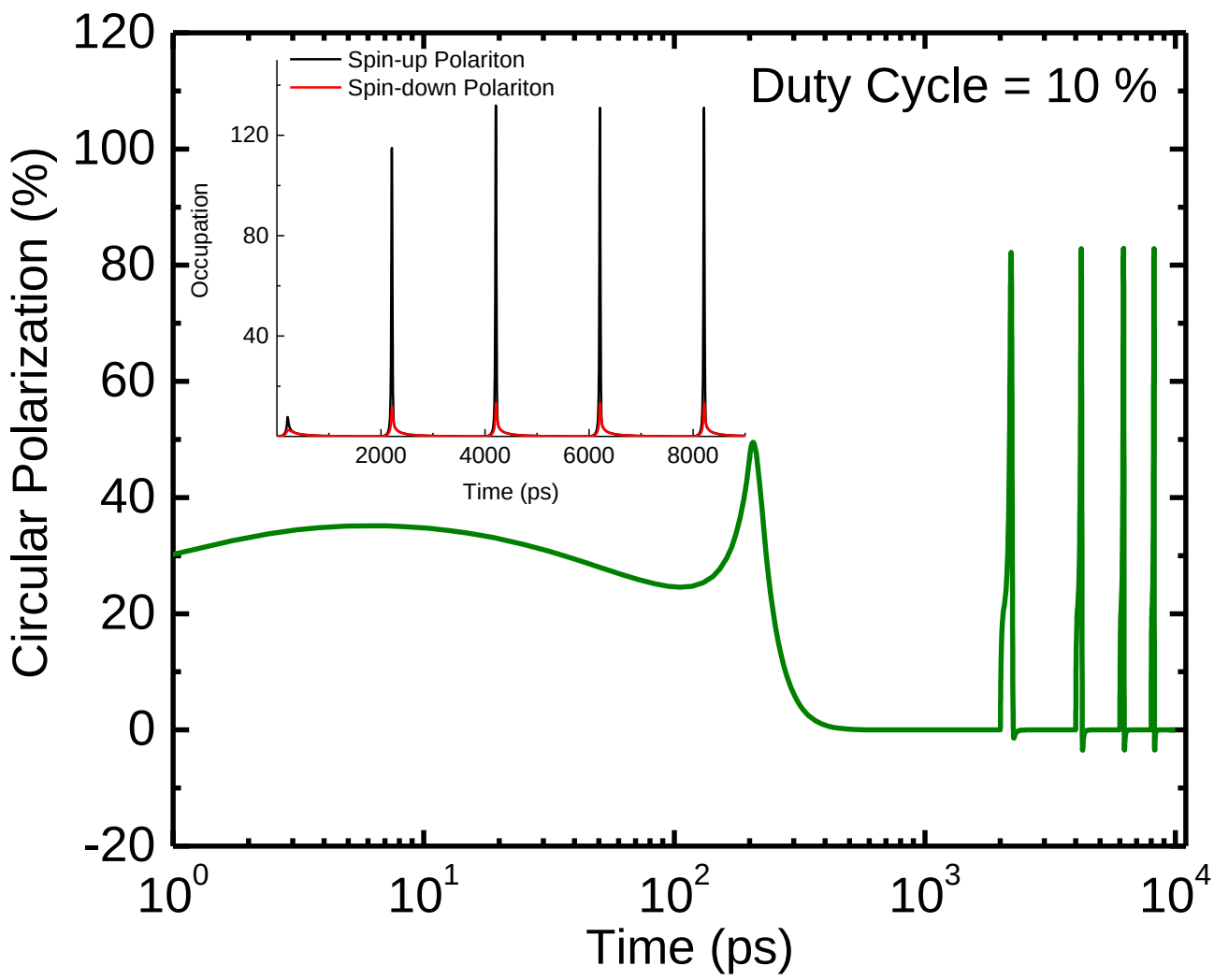

(b)

Figure 3 of 3